

Published by Cambridge University Press

This is an Open Access article, distributed under the terms of the Creative Commons Attribution licence (http://creativecommons.org/licenses/by/4.0/), which permits unrestricted re-use, distribution and reproduction, provided the original article is properly cited.

doi:10.1017/S002237782400059X

Nonlinear solution of classical three-wave interaction via finite-dimensional quantum model

Michael Q. May ¹⁰1,† and Hong Qin ¹⁰1

¹Princeton Plasma Physics Laboratory, Princeton University, Princeton, NJ 08540, USA

(Received 8 January 2024; revised 19 April 2024; accepted 22 April 2024)

The quantum three-wave interaction, the lowest-order nonlinear interaction in plasma physics, describes energy-momentum transfer between three resonant waves in the quantum regime. We describe how it may also act as a finite-degree-of-freedom approximation to the classical three-wave interaction in certain circumstances. By promoting the field variables to operators, we quantize the classical system, show that the quantum system has more free parameters than the classical system and explain how these parameters may be selected to optimize either initial or long-term correspondence. We then numerically compare the long-time quantum—classical correspondence far from the fixed point dynamics. We discuss the Poincaré recurrence of the system and the mitigation of quantum scrambling.

Keywords: quantum plasma, plasma nonlinear phenomena

1. Introduction

The three-wave interaction equations may describe the dynamics of the nonlinear interactions of three waves, or they can describe individual or pairs of small-amplitude waves in nonlinear media. For example, in the decay interaction, a large-amplitude wave with frequency ω_1 and wavenumber k_1 will decay into two smaller waves with energies ω_2 , ω_3 and wavenumbers k_2 , k_3 if the resonance conditions $\omega_1 = \omega_2 + \omega_3$ and $k_1 = k_2 + k_3$ are met. The three-wave interaction equations have applications in laser-plasma interactions (Moody *et al.* 2012; Myatt *et al.* 2014), determining weak turbulence spectra (Zakharov, L'vov & Falkovich 2012), nonlinear optical system design (Frantz & Nodvik 1963; Ahn *et al.* 2003; Brunton *et al.* 2012) and oceanic wave theory (Kadri & Stiassnie 2013). Although the three-wave equations are well studied (Rosenbluth, White & Liu 1973; Zakharov & Manakov 1976; Kaup, Reiman & Bers 1979; Reiman 1979) and their solutions (in terms of Jacobi elliptic functions, Armstrong *et al.* 1962) are known, the three-wave interaction equations provide a model for understanding nonlinear interactions in general, as they are the lowest-order nonlinear interactions found in many systems, including plasma physics.

† Email address for correspondence: mqmay@princeton.edu

Nonlinear dynamical systems often display complex behaviours, so, were the solution to the three-wave equations unknown, we may approach solving them via finite-difference integration of the system's Liouville equation (necessary if there is uncertainty in the initial condition). Because of the large computational cost this entails, many techniques have been developed to transform nonlinear systems into linear systems with a finite state space. The transformation to a finite, linear system also facilitates the use of quantum computers since quantum computers act on finite-dimensional spaces with linear operators. A popular technique is the process of Koopman embedding, initially developed by Koopman (1931) and von Neumann (1932) (KvN), in which the a nonlinear system is transformed into a (potentially) infinite-dimensional linear system using operational dynamics. This operational dynamic method allows for extensions of the Hartman-Grobman theorem, which shows that the linearized dynamics around fixed points will be qualitatively similar to the actual dynamics, to entire basins of attraction (Lan & Mezić 2013), and there may be significant computational advantages to evaluating classical dynamics rendered finite-dimensional by the KvN method on a quantum computer (Joseph 2020).

Operational dynamic methods have several significant drawbacks, however, which restrict their theoretical applications. For actual computation, the linear infinite-dimensional systems must be rendered finite, either by finding a Koopman-invariant subspace or using a closure. There is research into determining Koopman-invariant finite subspaces (Mezić & Wiggins 1999; Budišić & Mezić 2012; Brunton *et al.* 2016), but solutions are often narrowly tailored to specific systems. Operational dynamical methods also suffer from the issue of *ad hoc* linearization, with an infinite number of Koopman linearizations possible for most nonlinear systems. Although the original work of Koopman prescribed a unitary embedding, this has often been ignored in Koopman-derived research, particularly dynamical mode decomposition. Care must be taken to ensure that the linearization and closure chosen result in unitary linear dynamics for applications in quantum computation.

Instead of using operational dynamics to linearize the quantum three-wave interaction, we propose transforming the classical interaction into a quantum interaction via the quantum field-theoretic method, originally explored for the three-wave interaction by Shi, Qin & Fisch (2017), Shi (2018) and Shi, Qin & Fisch (2021b) and robustly simulated on a quantum computer (Shi et al. 2021a). In this method, the classical dynamic variables, which represent the waves' amplitudes, are promoted to linear operators which obey canonical commutation relations and act on a Hilbert space. If the resultant system is infinite-dimensional, as one would expect from a Koopman linearization, nothing would be gained from the quantization; however, it happens that, for the three-wave interaction, the quantization allows for a natively finite-dimensional description of the dynamics. Of course, this comes at the cost of the linear quantum system not necessarily capturing the classical nonlinear dynamics. The quantum wave function will not be localized, may be able to explore classically forbidden regions and will exhibit interference due to complex phase interactions. Despite these drawbacks, elsewhere, quantum versions of classical equations have been used to calculate classical dynamical quantities, including diffusion coefficients and Lyapunov exponents, more efficiently than the classical equations could (Benenti et al. 2001; Benenti, Casati & Montangero 2003; Joseph 2020).

Quantum-classical correspondence for the three-wave interaction has been previously explored in the context of quantum instabilities in non-chaotic classical systems (May & Qin 2023b), but this work was limited to linear time scales of less than one nonlinear orbit. In the following, we will use the quantum three-wave interaction as a model for the classical three-wave interaction, considering for the first time their relationship over

an entire nonlinear orbit. We find that that the quantum system is able to reproduce the classical nonlinear periodic solution for finite times. Thus, through its relationship with the classical three-wave interaction, the quantum three-wave interaction may serve as a fundamental model for the application of quantum field-theoretic quantization as a means of probing other nonlinear classical symplectic systems using linear unitary theory.

We begin in § 2 by reviewing the dynamics of the classical three-wave equations. We also review the formalism developed by Shi *et al.* for the quantum three-wave equations, including their finite state-space representation (Shi *et al.* 2017; Shi 2018; Shi *et al.* 2021*b*). We find that the governing equations of the classical and quantum interactions are structurally similar and discuss their differences. In § 3 we describe the initial conditions we will use for comparing the quantum and classical systems. We compare the integrated classical system with the finite, linear quantum system, finding excellent correspondence for many classical nonlinear periods. We also explain how hyperparameters available in the quantum system, including the initial variance and dimension, can be used to extend the correspondence between the quantum and classical systems, even for large nonlinearities. Finally in § 4, we summarize our findings and discuss their relevance to quantum computation.

2. Three-wave interactions

The homogeneous, classical three-wave equations for the decay interaction are given by

$$\partial_t A_1 = g A_2 A_3, \tag{2.1}$$

$$\partial_t A_2 = -g^* A_1 A_3^*, \tag{2.2}$$

$$\partial_t A_3 = -g^* A_1 A_2^*, \tag{2.3}$$

where A_j is the amplitude of the *j*th wave, A_j^* is its complex conjugate and *g* is the coupling coefficient (Jurkus & Robson 1960; Jaynes & Cummings 1963; Kaup *et al.* 1979; Reiman 1979). In addition to the Hamiltonian

$$H = gA_1^*A_2A_3 - g^*A_1A_2^*A_2^*, (2.4)$$

the interaction supports two other constants of motion

$$s_2 = I_1 + I_3, (2.5)$$

$$s_3 = I_1 + I_2, (2.6)$$

where $I_j = A_j^* A_j$ is the wave action of the *j*th wave. Because the wave amplitudes A_j are not real-valued, their quantum analogues will not be observables. Thus, to directly compare the classical and quantum three-wave interactions, we will consider the second-order differential equation for the first wave action

$$\partial_t^2 I_1 = 2|g|^2 (s_2 s_3 - 2(s_2 + s_3)I_1 + 3I_1^2), \tag{2.7}$$

which is obtained directly by differentiating I_1 and making substitutions using (2.1)–(2.3) and (2.5) and (2.6). The dynamics for I_2 and I_3 is the same as that for I_1 thanks to the constants s_2 and s_3 . Note that the second-order differential equation for I_1 is decoupled from the equations for I_2 and I_3 (which is not the case for the first-order differential equation for I_1). Because there is a symmetry between s_2 and s_3 , in what follows we will assume $s_3 \ge s_2$.

We can further simplify this equation by scaling it by s_2 and making the time parameter dimensionless so

$$\partial_{\tau}^{2}x = 2(c - 2(1+c)x + 3x^{2}), \tag{2.8}$$

with the scaled wave amplitude $x = I_1/s_2$, the constant $c = s_3/s_2$ and the time parameter $\tau = |g|\sqrt{s_2}t$. In this form, the three initial conditions $A_1(t=0)$, $A_2(t=0)$ and $A_3(t=0)$ necessary to integrate (2.1)–(2.3) become initial conditions on the first wave's scaled action x, $x(\tau=0)$, its first derivative, $\partial_{\tau}x(\tau=0)$, and the constant c. Equation (2.8) is integrable, and one solution can be written as a Jacobi elliptic function

$$x(\tau) = c \operatorname{sn}^{2}(p + \tau, c), \tag{2.9}$$

where p is a constant determined by the initial conditions. Note that, although (2.8) is a second-order equation, the above solution only has a single free parameter. This is because the solution space for (2.8) is much larger than that of the original problem given by (2.1)–(2.3), to which (2.9) is also a solution. The space of initial conditions $A_1(0)$, $A_2(0)$ and $A_3(0)$ is not surjective onto the space of c, x(0) and $\partial_{\tau}x(0)$. Indeed, because s_2 , a constant determined by the initial conditions, has been scaled out of (2.8), we are not free to determine x(0) and $\partial_{\tau}x(0)$ independently. There are additional requirements that $c \ge 1$ and $0 \le x(0) \le 1$. It is also clear from (2.8) that the constant c will act as the modulator of the nonlinearity of the interaction. Taking c = 1, its lowest value since we have assumed $s_3 \ge s_2$, maximizes the effect of the nonlinear term s_2 , while taking s_3 the system becomes linear and the Hamiltonian becomes that of the algebraic discrete quantum harmonic oscillator (May & Qin 2023 s_3).

Using the quantum field-theoretic method of quantization, we can promote the wave amplitudes of (2.1)–(2.3) to operators and replace the complex conjugation with Hermitian conjugation to obtain a set of quantum three-wave equations

$$\partial_{t}\hat{A}_{1} = g\hat{A}_{2}\hat{A}_{3},
\partial_{t}\hat{A}_{2} = -g^{*}\hat{A}_{1}\hat{A}_{3}^{\dagger},
\partial_{t}\hat{A}_{3} = -g^{*}\hat{A}_{1}\hat{A}_{2}^{\dagger}.$$
(2.10)

The operators have the canonical commutation relations $[\hat{A}_j, \hat{A}_k^{\dagger}] = \delta_{j,k}$ for $j, k \in \{1, 2, 3\}$ and with $\delta_{j,k}$ the Kronecker delta function. The quantum Hamiltonian

$$\hat{H} = ig\hat{A}_{1}^{\dagger}\hat{A}_{2}\hat{A}_{3} - ig^{*}\hat{A}_{1}\hat{A}_{2}^{\dagger}\hat{A}_{3}^{\dagger}, \tag{2.11}$$

and the mutually commuting operators

$$\hat{s}_2 = \hat{n}_1 + \hat{n}_3,\tag{2.12}$$

$$\hat{s}_3 = \hat{n}_1 + \hat{n}_2, \tag{2.13}$$

where the number operators are defined in the usual way, $\hat{n}_j = \hat{A}_j^{\dagger} \hat{A}_j$. We will denote the eigenvalues of these Hermitian operators with the same symbols as the classical operators, e.g. $\langle \hat{s}_2 \rangle = s_2$. As found by Yuan Shi (Shi *et al.* 2021*a*), eigenvectors of the operators \hat{s}_2 and \hat{s}_3 , and the eigenvectors of the number operators \hat{n}_1 , \hat{n}_2 and \hat{n}_3 form a finite $d = s_2 + 1$ -dimensional invariant subspace when acted on by the Hamiltonian. We can

write such subspace elements as

$$\Psi(t) = \sum_{i=0}^{s_2} \alpha_j(t) \psi_j,$$
 (2.14)

where

$$\psi_i = |s_2 - i, s_3 - s_2 + i, i\rangle,$$
 (2.15)

has eigenvalues $\{\hat{n}_1, \hat{n}_2, \hat{n}_3\}\psi_j = \{s_2 - j, s_3 - s_2 + j, j\}\psi_j$. The finiteness of the subspace may be directly seen through the action of the Hamiltonian on a subspace element ψ_j :

$$H\psi_{j} = ig(s_{2} - j + 1)^{1/2}(s_{3} - s_{2} + j)j^{1/2}\psi_{j-1} - ig^{*}(s_{2} - j)^{1/2}(s_{3} - s_{2} + 1 + j)(j + 1)^{1/2}\psi_{j+1}.$$
(2.16)

If $j = s_2$ in the above equation, then the coefficient of ψ_{s_2+1} will be zero and similarly for j = 0 and ψ_{-1} . The action of the Hamiltonian on these subspace elements can be calculated directly from the Schrödinger equation

$$i\partial_{\tau}\Psi = H\Psi,$$
 (2.17)

where we have taken the constant $\hbar = 1$. Writing $\Psi(t)$ as a column vector of weights $(\alpha_0(t), \alpha_1(t), \dots \alpha_s, (t))$, H becomes a $d \times d$ tridiagonal matrix,

$$H = \begin{pmatrix} 0 & h_0 & 0 & 0 & 0 & \dots \\ h_0 & 0 & h_1 & 0 & 0 & \dots \\ 0 & h_1 & 0 & h_2 & 0 & \dots \\ 0 & 0 & h_2 & 0 & h_3 & \dots \\ \vdots & \vdots & \vdots & \vdots & \vdots & \ddots \end{pmatrix}, \tag{2.18}$$

with

$$h_j = \sqrt{(s_2 - j)(s_3 - s_2 + 1 + j)(j + 1)}. (2.19)$$

Thus, explicitly, we may write the Schrödinger equation as a system of d coupled first-order linear differential equations:

$$i\dot{\alpha}_0 = h_0 \alpha_1,\tag{2.20}$$

$$i\dot{\alpha}_1 = h_0\alpha_0 + h_1\alpha_2,\tag{2.21}$$

. .

$$i\dot{\alpha}_{i} = h_{i-1}\alpha_{i-1} + h_{i}\alpha_{i+1}.$$
 (2.22)

We have taken g = -i in the above equations for simplicity; however, it will be shown that the phase and magnitude of g will not affect the quantum dynamics, as they did not affect the classical scaled dynamics of (2.8), below. Note that many efficient techniques have been developed for simulating sparse Hamiltonian dynamics, such as that of (2.20)–(2.22), on quantum computers. See, for example, Berry *et al.* (2015) and Low & Chuang (2017).

To compare this finite linear system with the nonlinear classical system, we need only take the expectation value of \hat{n}_1

$$\langle \hat{n}_1 \rangle = \sum_{i=0}^{s_2} |\alpha_j|^2 (s_2 - j),$$
 (2.23)

and compare it with the classical wave action I_1 . Of course, the quantum linear dynamical equations and the classical nonlinear equations refer to different systems, so their

dynamics will diverge except in the classical limit ($s_2 \to \infty$). Let us find the quantum equivalent of the classical (2.8) to see how the quantum dynamics might be written as a nonlinear differential equation. First, we find a second-order equation for \hat{n}_1 by using the quantum three-wave equations and making substitutions with the definitions of \hat{s}_2 and \hat{s}_3 :

$$\partial_t^2 \hat{n}_1 = 2|g|^2 (\hat{s}_2 \hat{s}_3 - (2\hat{s}_2 + 2\hat{s}_3 + 1)\hat{n}_1 + 3\hat{n}_1^2). \tag{2.24}$$

This is similar to that for I_1 in (2.7). Next, we take the expectation of this equation

$$\partial_t^2 \langle n_1 \rangle = 2|g|^2 (s_2 s_3 - (2s_2 + 2s_3 + 1)\langle n_1 \rangle + 3\langle n_1 \rangle^2 + 3\delta), \tag{2.25}$$

where we have defined the variance

$$\delta = \langle n_1^2 \rangle - \langle n_1 \rangle^2. \tag{2.26}$$

Finally, we scale the equation for $\langle \hat{n}_1 \rangle$ by s_2^2 , make the equation dimensionless by using the time parameter to absorb the coupling coefficient g and define $x_Q = \langle n_1 \rangle / s_2$, $\tau = |g| \sqrt{s_2} t$, and $\delta' = \delta / s_2^2$ to arrive at

$$\partial_{\tau}^{2} x_{Q} = 2\left(c - 2\left(1 + c + \frac{1}{2s_{2}}\right)x_{Q} + 3x_{Q}^{2} + 3\delta'\right),\tag{2.27}$$

which may be directly compared with (2.8). Both the quantum equation for x_Q and the classical (2.8) for x are the same except for the additional linear factor of $2x_Q/s_2$ and the inclusion of the scaled variance in the quantum system. As the dimension of the quantum system increases, so will s_2 , diminishing the effect of the $2x_Q/s_2$ term; however, the effect of the variance in (2.27) will depend on the initial conditions of the quantum system, not just the total dimension. Also, note the variance is not a function of x_Q . It must be calculated directly from the Schrödinger equation.

3. Quantum-classical correspondence

The initial conditions of the quantum system must be chosen carefully to correspond to those in the classical system. Consider an arbitrary initial condition where we write the weights of (2.23) in polar form

$$\alpha_j = r_j \,\mathrm{e}^{\mathrm{i}\phi_j},\tag{3.1}$$

with a real amplitude r_j and argument ϕ_j . Using (2.20)–(2.22), we may directly differentiate (2.23) to find

$$\partial_t \langle \hat{n}_1(0) \rangle = 2 \sum_{j=0}^{s_2} h_j r_j r_{j+1} \sin(\phi_{j+1} - \phi_j).$$
 (3.2)

In choosing the initial condition for the classical system, for exact correspondence we would have $x(0) = x_Q(0)$, $\partial_\tau x(0) = \partial_\tau x_Q(0)$ and the nonlinearity parameters equal. This system of equations is underdetermined, however, because the quantum system has many more degrees of freedom, $f \sim O(s_2)$, than the classical system. To deal with this, we will restrict ourselves to considering quantum initial conditions for which the real amplitude r_j is taken to be a Gaussian over the index of α_j with a mean μ and standard deviation σ which will depend on the dimension of the quantum system

$$r_j = \mathcal{N} \exp\left(-\frac{(j - \mu s_2)^2}{2\sigma^2}\right). \tag{3.3}$$

The normalization \mathcal{N} must account for the initial condition being clipped since $r_{-1} = r_{s_2+1} = 0$. Note that the initial scaled variance δ'_0 of the quantum system is only

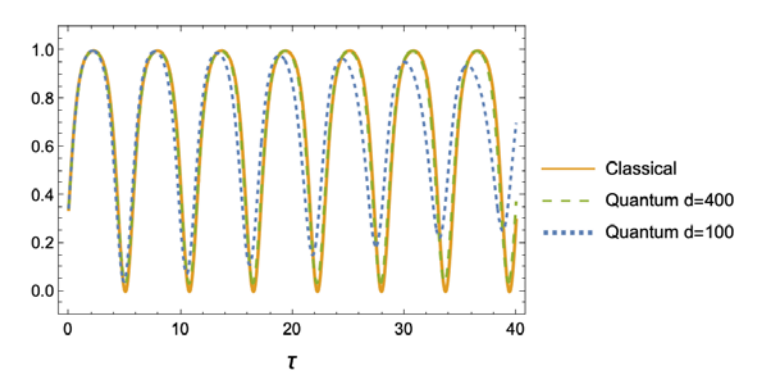


FIGURE 1. Comparison between nonlinear classical and quantum dynamics. The initial standard deviation chosen for the quantum systems is set at d/5, and the nonlinearity parameter c = 1.05.

qualitatively related to the standard deviation σ since

$$\delta_0' = \left(\sum_{j=0}^{s_2} r_j^2 (1 - j/s_2)^2\right) - \left(\sum_{j=0}^{s_2} r_j^2 (1 - j/s_2)\right)^2,\tag{3.4}$$

while

$$\sigma = \left(\sum_{j=0}^{s_2} r_j^2 (j-\mu)^2 - \left(\sum_{j=0}^{s_2} r_j^2 (j-\mu)\right)^2\right)^{1/2}.$$
 (3.5)

Let us further restrict our quantum initial conditions to those which are velocity maximizing, which amounts to taking $\phi_{j+1} - \phi_j = \pi/2$ for all j. This is a prescription of the initial phase of the quantum nonlinear orbit. Since we are principally interested in correspondence over the course of many nonlinear orbits, the initial phase should not matter for our analysis. We thus need to match μ and σ for the point on the classical orbit where the velocity is maximized. As noted in § 2, x(0) and $\partial_{\tau}x(0)$ are not independent, so choosing to maximize the classical velocity also specifies a point on the classical trajectory. The solution to (2.8) at the classical inflection point (when $\partial_{\tau}^2 x = 0$) is

$$x_0 = \frac{1}{2}(1 + c - \sqrt{1 + c^2 - c}). \tag{3.6}$$

The negative root is chosen because the velocity at the inflection point

$$\dot{x}_0 = 2\sqrt{x_0}\sqrt{1 - x_0}\sqrt{c - x_0} \tag{3.7}$$

becomes imaginary for the positive root. Finally, we set $\mu = x_0$. The choice of initial standard deviation σ will be discussed below.

We compare the integrated classical system with initial conditions $x(0) = x_0$, $\partial_{\tau}x(0) = \dot{x}_0$ with the quantum system in figures 1, 2 and 8. As discussed above, the initial condition is Gaussian in r, and we have also taken $\mu = x_0$, $\sigma = d/5$ and the normalization \mathcal{N} chosen such that the total probability is 1. In what remains of this section, we will consider the quantum-classical correspondence and various effects on that correspondence due to different choices of nonlinearity parameter c, the initial standard deviation σ and the quantum dimension d.

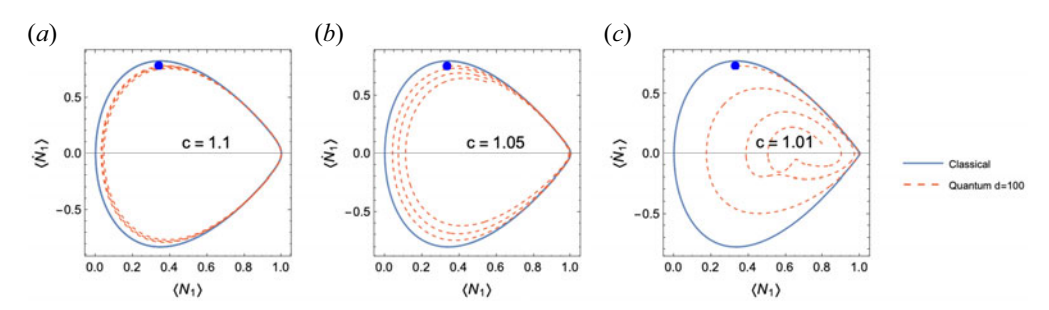


FIGURE 2. Phase-space plots of the classical (x, \dot{x}) and quantum (x_Q, \dot{x}_Q) systems with initial condition (x_0, \dot{x}_0) , initial quantum dimension d=100 and initial quantum standard deviation $\sigma=20$ for three values of the nonlinearity parameter, c=1.1, 1.05 and 1.01. The classical trajectories are shown in solid blue lines. The quantum trajectories are shown via the dashed red lines. The blue dot indicates the initial condition. Each system is evolved for three classical orbits.

In figure 1, we compare three systems, two quantum with d=100 and d=400 and the classical system, for a nonlinearity parameter c=1.05. Recall that $c\geq 1$, and as $c\to 1$, the nonlinearity increases. Despite the quantum and classical velocities being independently maximized, there is excellent initial correspondence between all three systems. The nonlinearity is pronounced enough that the d=100 system diverges from the classical solution within a couple of periods; however, the correspondence for the d=400 system lasts much longer, with the d=400 quantum system accurately capturing both the nonlinearity of the classical orbit as well as its period.

We may more carefully explore the effect of the nonlinearity parameter c on the quantum-classical dynamics via phase-space diagrams of the quantum d = 100 and classical systems in figure 2. Three classical nonlinear orbits are shown for each of the nonlinearity parameters c = 1.1, 1.05 and 1.01. Decreasing the nonlinearity parameter causes the classical orbits to become more pinched. This increasingly linear relationship between $\langle \hat{n}_1 \rangle$ and $\partial_{\tau} \langle \hat{n}_1 \rangle$ indicates exponential-like growth, the onset of the classical instability and its quantum counterpart (see May & Qin 2023b). From the quantum orbits in figure 2, it is obvious that, as the nonlinearity increases, the correspondence between the systems decreases. Investigations into exponential growth of quantum correlators in non-chaotic systems indicate that proximity to the classical fixed point leads to quantum scrambling (Xu, Scaffidi & Cao 2020). For instance, after a single pass near the classical fixed point, the d = 100 system sharply diverges from the classical solution for c = 1.01. On the other hand, the d = 100 quantum system approximates the classical solution for a couple of classical periods for c = 1.05 (see also figure 1), and the correspondence lasts for much longer for c = 1.1. The proximate cause of the sharp divergence of the quantum system from the classical system near the fixed point is the increased classical period as $c \to 1$. Since the quantum system may only approximate the classical system for finite times, when $c \to 1$ and the classical period tends to infinity, the quantum solution will inevitably diverge from the classical solution within a single period.

Shown in figure 3 is the error as a function of the dimension of the quantum system for a nonlinearity parameter c=1.05. The error is calculated by averaging the absolute value of the difference between the classical and quantum systems over a single classical period. The log of this mean absolute error (MAE) is shown for each of the first four classical periods. Note that, for two uncorrelated oscillators with amplitude 1, the expected value of the MAE will be 0.25. A MAE higher than this must be due to anti-correlated phases.

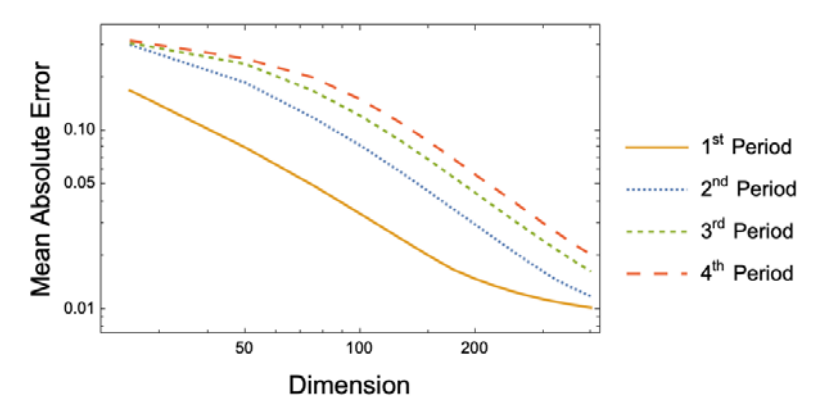


FIGURE 3. Log-log plot of the MAE between the classical and quantum systems with c=1.05, averaged over each of the first four classical periods. The dimension d ranges from 25 to 400.

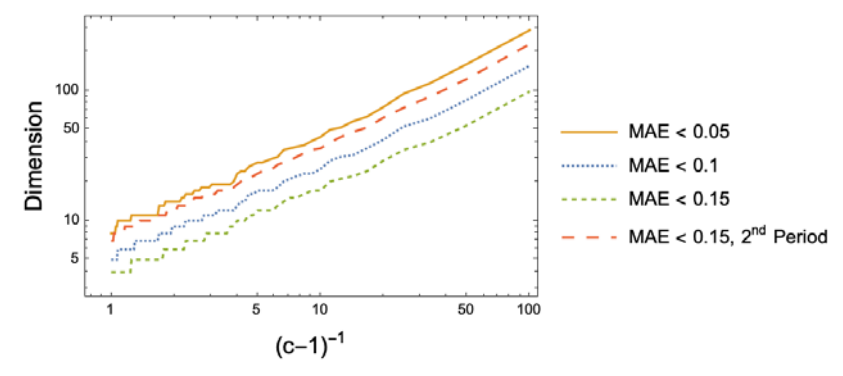


FIGURE 4. Log-log plot of the dimension versus the transformed nonlinearity parameter $c' = (c-1)^{-1}$ for various values of the MAE between the quantum and classical solutions during the first and second classical periods. The threshold error values for the first classical period are 0.15, 0.1 and 0.05. Also shown, in the red, large dashes, is the dimension necessary to keep the MAE below 0.15 during the second classical period. The original nonlinearity parameter c ranges from 2 (highly linear, left side of the plot) to 1.01 (highly nonlinear, right side of the plot).

This occurs for low dimension in figure 3. As the dimension of the quantum simulation is increased, the error decays exponentially. There is a minimum error, however, which may be attributed to our choice of initial conditions, particularly the initial standard deviation.

For a target value of the MAE, how does the dimension scale with increasing nonlinearity? Recall that the nonlinearity parameter ranges from 1, when the nonlinearity is maximized, to ∞ , where the nonlinearity disappears. For clarity, we make the transformation $c' = (c-1)^{-1}$, so that $c' \in (0, \infty)$, and increasing c' increases the nonlinearity. In figure 4, we show how the dimension depends on c' for various target values of the MAE between the quantum and classical solutions for either the first or second classical period. For each value of the threshold error, the slope is remarkably consistent. This consistency is not limited to the short time scales either: looking at how the dimension scales with c' for a threshold error of 0.15 during the second period, we see the same slope. We can approximate this exponential relationship

$$d \propto (c-1)^{\gamma} \tag{3.8}$$

with $\gamma \sim -3/4$.

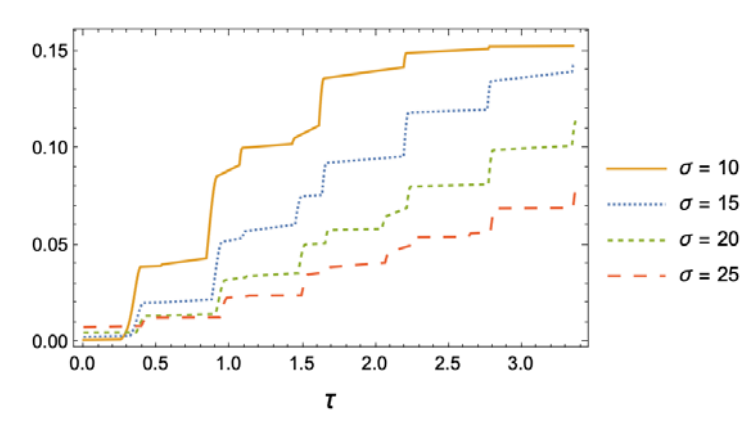


FIGURE 5. Maximum variance over time for the d = 200, c = 1.05 quantum three-wave interaction. Results for various initial standard deviations are shown.

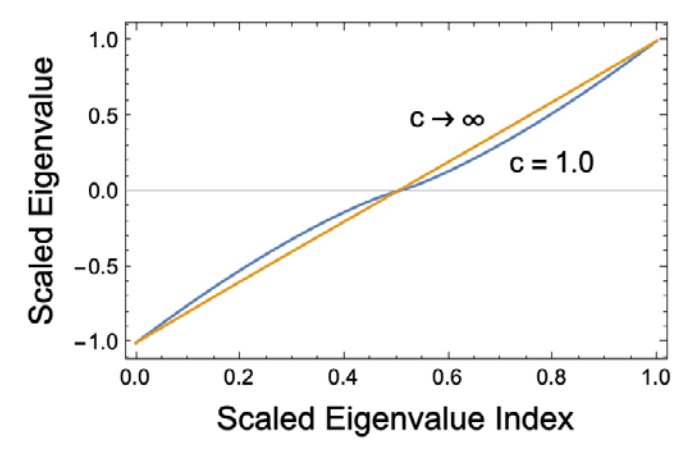


FIGURE 6. Eigenvalues of the Hamiltonian scaled by the highest eigenvalue. The indices of the eigenvalues linearly increase from that of the lowest eigenvalue 0, to the highest index 1. For finite-dimensional systems, the eigenvalues will lie between the c=1 and $c\to\infty$ curves.

So far, the initial standard deviation of the quantum system has been taken to be $\sigma=d/5$ for simplicity; however, this does not necessarily lead to the best correspondence with the classical system. There is a trade off between long-term fidelity and the size of the initial variance. Shown in figure 5 is the growth of the variance over time given different initial standard deviations. Only the maximum variance is plotted because the magnitude of the variance oscillates with the amplitude of the wave. This can be seen in the spurts of growth of the maximum variance occurring at multiples of the period of the nonlinear oscillation. For a higher initial standard deviation, the variance grows more slowly with time.

The slow growth of the variance with larger initial standard deviations is attributable to the spectrum of the Hamiltonian, shown in figure 6. When $c \to \infty$, the d eigenvalues will be exactly linearly distributed, and for finite c > 1, they will lie between the two lines of the figure. Importantly, even for the maximally nonlinear c = 1, the eigenvalues with small absolute value (those with scale eigenvalue indices of around 0.5) will still be approximately linearly distributed. As the three-wave interaction acts similarly to a

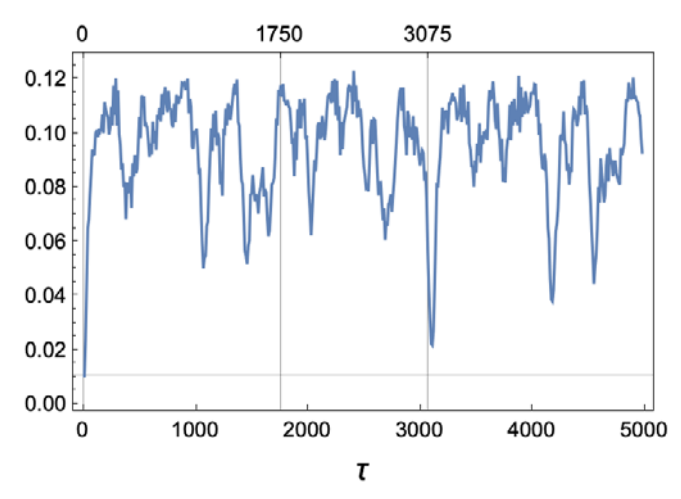


FIGURE 7. Variance of d=100 quantum system with nonlinearity parameter c=1.05 and initial standard deviation set to $\sigma=d/5=20$. The three labelled vertical gridlines at $\tau=0$, 1750 and 3075 indicate the starting times of the three elements of figure 8. The horizontal gridline shows the starting variance $\delta'=0.011$.

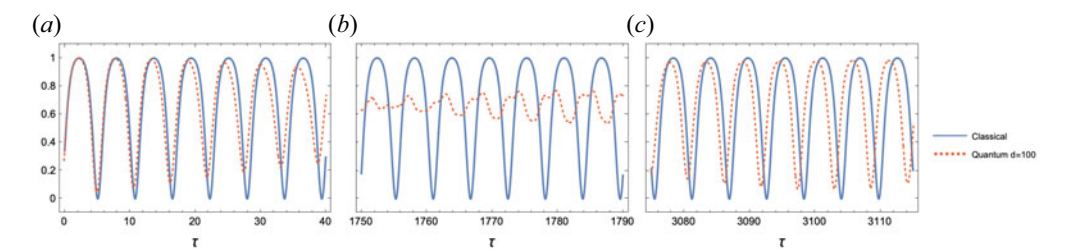


FIGURE 8. Comparison between classical and quantum dynamics for nonlinearity parameter c=1.05 beginning at three times $\tau=0$, 1750 and 3075. The plot beginning at $\tau=1750$ typifies high variance behaviour, and the plot beginning at time $\tau=3075$ shows a partial quantum revival, which was found by looking for relative minima in the variance of figure 7. The d=100 quantum system begins with a standard deviation of $\sigma=d/5=20$.

perturbed quantum harmonic oscillator, we may by analogy understand that states with a large initial standard deviation are represented by the lowest energy eigenmodes—those eigenmodes which reside in the central, linear area of figure 6. With higher initial variance states having their dominant eigenfrequencies linearly distributed, they remain in correspondence with the classical dynamics for longer periods of time. Thus, despite a high initial variance coming at the cost of the quantum (2.27) beginning with a dynamics farther from that of the classical (2.8) with no variance, the effect of quantum interference is suppressed. Of course, if the initial variance is taken to be too large, (i) the initial condition may no longer be taken to be Gaussian, and (ii) the initial condition ceases to be well-approximated by lower-frequency eigenstates. An initial standard deviation of $\sigma = d/5$ strikes a balance between the need for a small growth rate of the variance with the need to prevent clipping of the initial Gaussian in the finite domain with $\alpha_{-1} = \alpha_d = 0$ enforced.

The variance may be used as a tool to determine where quantum revivals will occur. Shown in figure 7 is the variance for the d = 100 quantum system for the

first approximately 880 classical orbits. The initial standard deviation is $\sigma=20$, which corresponds to an initial variance of $\delta'=0.011$. Beginning around $\tau=3075$, the variance sharply decreases to a minimum of $\delta'=0.022$, indicating a partial quantum revival, shown in figure 8. Although the phase and amplitude of the quantum system differ from those of the classical, during the revival, the quantum system accurately captures the period of the classical orbit. When the variance is higher, for example, beginning at $\tau=1750$, it is difficult to characterize the correlation between the quantum and classical systems.

4. Conclusions

As a model for the classical system, the quantum description of the three-wave interaction has several advantages. First, via the correspondence principle, the classical and quantum systems are guaranteed to converge as the dimension of the quantum system is increased. Second, we did not need to rely on closures or arbitrary choices of a finite representation, as would have been the case for a KvN quantization of the classical dynamics. The quantum field-theoretic method for quantization provides a systematic means of rendering the dynamics discrete, finite-dimensional and unitary. Finally, as displayed in figures 1 and 3, the quantum system of appropriate dimension can capture both the qualitative and quantitative aspects of the nonlinear periodic solution, including its frequency.

While the dimension of the quantum systems being compared with classical dynamics has been large ($d \sim 100$), simulations of this degree may soon be achievable with quantum computers. Since $n \propto \log_2(d)$, where n is the number of qubits necessary to represent a state, neglecting error correction, a d=100 quantum state only requires 8 qubits to represent it. However, difficulties would arise from approximating the three-wave Hamiltonian as a series of universal gates acting on those qubits. In general, approximating arbitrary unitary operators can require $O(d^2)$ gate applications, which is obviously untenable for high dimension. Shi *et al.*, in simulations of the quantum three-wave equations with d=3, have shown this problem may be sidestepped, however, through the creation of special-made gates particular to the system one is simulating (Shi *et al.* 2021*a*).

Another hurdle to quantum simulation of the three-wave interaction is quantum state preparation. Initializing a non-sparse arbitrary state, which would include our Gaussian initial state, may require either an exponential (in the number of qubits n, so linear in the dimension d) number of operations (Plesch & Brukner 2011) or an exponential number of ancillary qubits (Zhang, Li & Yuan 2022).

Finally, we should consider the information being extracted from the quantum system. Measuring the full time history of each component of the quantum phase space, α_i , will destroy any potential quantum speedup; however, when compared with simulating the full classical Liouville dynamics, simulating the quantum dynamics may result in speedups as long as the extracted information is sparse. In particular, we have shown that low-dimensional classical information, including the nonlinear frequency and the expectation value of the number operator, may be effectively simulated in a quantum system. While the three-wave interaction is only the lowest-order nonlinearity in plasma physics, this opens the possibility of using natively unitary quantum dynamics to model more complicated classical, nonlinear dynamics on quantum hardware in the near future.

Acknowledgements

Editor Thierry Passot thanks the referees for their advice in evaluating this article.

Funding

This research was supported by the U.S. Department of Energy (DE-AC02-09CH11466).

Declaration of interests

The authors report no conflict of interest.

REFERENCES

- AHN, J., EFIMOV, A., AVERITT, R. & TAYLOR, A. 2003 Terahertz waveform synthesis via optical rectification of shaped ultrafast laser pulses. *Opt. Express* 11, 2486.
- ARMSTRONG, J.A., BLOEMBERGEN, N., DUCUING, J. & PERSHAN, P.S. 1962 Interactions between light waves in a nonlinear dielectric. *Phys. Rev.* 127, 1918.
- BENENTI, G., CASATI, G. & MONTANGERO, S. 2003 Quantum computing and information extraction for dynamical quantum systems. In *Experimental Aspects of Quantum Computing* (ed. Henry O. Everitt), pp. 273–293, Springer.
- BENENTI, G., CASATI, G., MONTANGERO, S. & SHEPELYANSKY, D.L. 2001 Efficient quantum computing of complex dynamics. *Phys. Rev. Lett.* 87, 227901.
- BERRY, D.W., CHILDS, A.M., CLEVE, R., KOTHARI, R. & SOMMA, R.D. 2015 Simulating hamiltonian dynamics with a truncated taylor series. *Phys. Rev. Lett.* **114**, 090502.
- BRUNTON, G., ERBERT, G., BROWNING, D. & TSE, E. 2012 The shaping of a national ignition campaign pulsed waveform. *Fusion Engng Des.* 87, 1940.
- BRUNTON, S.L., BRUNTON, B.W., PROCTOR, J.L. & KUTZ, J.N. 2016 Koopman invariant subspaces and finite linear representations of nonlinear dynamical systems for control. *PLoS ONE* **11** (2), e0150171.
- BUDIŠIĆ, M. & MEZIĆ, I. 2012 Geometry of the ergodic quotient reveals coherent structures in flows. *Physica* D **241** (15), 1255–1269.
- FRANTZ, L. & NODVIK, J. 1963 Theory of pulse propagation in a laser amplifier. *J. Appl. Phys.* **34**, 2346. JAYNES, E.T. & CUMMINGS, F.W. 1963 Comparison of quantum and semiclassical radiation theories with application to the beam maser. *Proc. IEEE* **51** (1), 89–109.
- JOSEPH, I. 2020 Koopman–von Neumann approach to quantum simulation of nonlinear classical dynamics. *Phys. Rev. Res.* **2**, 043102.
- JURKUS, A. & ROBSON, P.N. 1960 Saturation effects in a travelling-wave parametric amplifier. *Proc. IEE* B **107** (32), 119.
- KADRI, U. & STIASSNIE, M. 2013 Generation of an acoustic-gravity wave by two gravity waves, and their subsequent mutual interaction. *J. Fluid Mech.* **735**, R6.
- KAUP, D.J., REIMAN, A. & BERS, A. 1979 Space-time evolution of nonlinear three-wave interactions. I. Interaction in a homogeneous medium. *Rev. Mod. Phys.* **51** (2), 275–309.
- KOOPMAN, B.O. 1931 Hamiltonian systems and transformations in Hilbert space. *Proc. Natl Acad. Sci. USA* 17 (5), 315–318.
- LAN, Y. & MEZIĆ, I. 2013 Linearization in the large of nonlinear systems and Koopman operator spectrum. *Physica* D **242** (1), 42–53.
- LOW, G.H. & CHUANG, I.L. 2017 Optimal hamiltonian simulation by quantum signal processing. *Phys. Rev. Lett.* 118, 010501.
- MAY, M. & QIN, H. 2023a Algebraic discrete quantum harmonic oscillator with dynamic resolution scaling. arXiv:2304.01486.
- MAY, M. & QIN, H. 2023b The quantum three-wave instability. Phys. Rev. A 107, 062204.
- MEZIĆ, I. & WIGGINS, S. 1999 A method for visualization of invariant sets of dynamical systems based on the ergodic partition. *Chaos* **9** (1), 213–218.
- MOODY, J., et al. 2012 Multistep redirection by cross-beam power transfer of ultrahigh-power lasers in a plasma. *Nat. Phys.* **8**, 344.
- MYATT, J., et al. 2014 Multiple-beam laser-plasma interactions in inertial confinement fusion. *Phys. Plasmas* 21, 055501.
- PLESCH, M. & BRUKNER, C. 2011 Quantum-state preparation with universal gate decompositions. *Phys. Rev.* A 83, 032302.

- REIMAN, A. 1979 Space-time evolution of nonlinear three-wave interactions. II. Interaction in an inhomogeneous medium. *Rev. Mod. Phys.* **51** (2), 311–330.
- ROSENBLUTH, M., WHITE, R. & LIU, C. 1973 Temporal evolution of a three-wave parametric instability. *Phys. Rev. Lett.* **31**, 1190.
- SHI, Y. 2018 Plasma physics in strong field regimes. PhD thesis, Princeton University.
- SHI, Y., et al. 2021a Simulating non-native cubic interactions on noisy quantum machines. Phys. Rev. A 103, 062608.
- SHI, Y., QIN, H. & FISCH, N.J. 2017 Three-wave scattering in magnetized plasmas: from cold fluid to quantized Lagrangian. *Phys. Rev.* E **96** (2), 023204.
- SHI, Y., QIN, H. & FISCH, N.J. 2021b Plasma physics in strong-field regimes: theories and simulations. *Phys. Plasmas* **28** (4), 042104.
- VON NEUMANN, J.V. 1932 Zur operatorenmethode in der klassischen mechanik. *Ann. Math.* **33** (3), 587–642.
- Xu, T., Scaffidi, T. & Cao, X. 2020 Does scambling equal chaos? Phys. Rev. Lett. 124, 140602.
- ZAKHAROV, V., L'VOV, V. & FALKOVICH, G. 2012 Kolmogorov Spectra of Turbulence 1: Wave Turbulence. Springer.
- ZAKHAROV, V. & MANAKOV, S. 1976 The theory of resonance interaction of wave packets in nonlinear media. Sov. Phys. JETP 42, 842.
- ZHANG, X.-M., LI, T. & YUAN, X. 2022 Quantum state preparation with optimal circuit depth: implementations and applications. *Phys. Rev. Lett.* **129**, 230504.